# Proteome analyses reveal Endoplasmic Reticulum stress-induced changes in protein abundance associated with Ube2j2 deficiency in human cell culture

Dahlberg, C. L.[1,2,*], Zinkgraf, M.[2,*], Laugesen, S.H.[1], Søltoft, C.L.[1], Ginebra, Q.[1], Bennett, E.P.[3], Hartmann-Petersen, R.[1], and Ellgaard, L.[1,*]

Affiliations:

[1] Department of Biology, Linderstrøm-Lang Centre for Protein Science, University of Copenhagen, Copenhagen 2200, Denmark

[2] Department of Biology, Western Washington University, Bellingham, Washington, USA, 98225

[3] Genome Editing Department, Nucleic Acid Research, Novo Nordisk A/S, Måløv 2760, Denmakr

*Corresponding authors: Dahlberg, C. (dahlbec@wwu.edu), Zinkgraf, M. (zinkgrm@wwu.edu), Ellgaard, L. (lellgaard@bio.ku.dk)

Running title: Proteomic analysis of cells lacking Ube2j2

Keywords: Ube2j2, unfolded protein response, ER-associated degradation, ubiquitin proteasome system, protein degradation, E2 ubiquitin-conjugating enzyme, proteomics

## Abstract

The unfolded protein response (UPR) helps reinstate cellular proteostasis upon an accumulation of misfolded proteins in the endoplasmic reticulum (ER), in part through ER-associated degradation (ERAD). Ube2j2 is an ER-localized E2 ubiquitin-conjugating enzyme that participates in ERAD. We used mass spectrometry analysis of cultured U2OS cells to investigate how the loss of Ube2j2 affects the cellular proteome in response to tunicamycin-induced ER stress. We constructed a network of twelve statistically distinct modules of protein abundance profiles across conditions. We describe the Gene Ontology annotations for each module along with the "hub gene" proteins whose abundance levels most closely adhere to each module's protein abundance profile. Our analysis identifies known Ube2j2-associated pathways (e.g., the UPR and ERAD) and cellular functions that were previously unassociated with Ube2j2 (e.g., RNA metabolism, ER-Golgi transport, and cell-cycle progression). These data are available via ProteomeXchange with identifier PXD076153 and provide avenues for further investigation into the cellular functions of Ube2j2 under basal and ER-stressed conditions.

## Introduction

Protein ubiquitylation plays a central role in cell physiology by regulating a vast number of protein activities. The ubiquitin-proteasome system is well-established as a central axis for regulating targeted protein abundance, and it is also crucial in maintaining protein homeostasis (proteostasis) in conjunction with molecular chaperones. The general structure of interactions in the "ubiquitin cascade" utilizes increasing specificity to ensure that substrates are ubiquitylated properly. In mammalian cells, two E1 ubiquitin-activating enzymes are responsible for the ATP-dependent charging of ubiquitin, which is then transferred to one of approximately 40 E2 ubiquitin-conjugating enzymes (E2s) (van Wijk and Timmers 2010; Parashar et al. 2025). Ubiquitin-charged E2s interact directly with unique combinations of the hundreds of E3 ubiquitin-protein ligases (E3s) to transfer ubiquitin onto substrate molecules (Ye and Rape 2009; Stewart et al. 2016; Gundogdu and Walden 2019). Ubiquitylation can also be reversed by deubiquitylating enzymes (DUBs) (Fischer 2003; Sowa et al. 2009). Depending on the number and pattern of ubiquitin modifications, substrate proteins may be re-localized, activated, repressed, or degraded. Thus, specific cohorts of E2 conjugases and E3 ligases can have wide-ranging effects on cellular pathways.

E2 enzymes provide an initial element of subcellular and temporal regulation to the ubiquitylation cascade through spatial restriction (van Wijk et al. 2009; Ye and Rape 2009; van Wijk and Timmers 2010; Witus et al. 2021). E2s with specific subcellular localizations like the endoplasmic reticulum (ER), cytosol, nucleus, or mitochondria, are positioned to interact with E3 ligases to facilitate ubiquitylation of more narrowly defined classes or groups of proteins (Stewart et al. 2016; Christianson and Carvalho 2022). Nonetheless, some E3-containing complexes, such as those that function in ER-associated degradation (ERAD), target diverse groups of substrates (Carvalho et al. 2006; Ravid et al. 2006; Sato et al. 2009; Sharninghausen et al. 2024) despite being spatially constrained.

The ERAD machinery is transcriptionally controlled downstream of the Unfolded Protein Response (UPR), which coordinates transcriptional and translational responses to proteotoxic stress caused by e.g., protein misfolding and aggregation, hypoxia, and oxidative stress (reviewed in Hetz et al., 2015). The overall aim of the UPR is to reinstate cellular homeostasis and, should this fail, initiate apoptosis. ERAD complexes identify and remove misfolded proteins from the ER lumen and membrane and target them for degradation by the proteasome (reviewed in Christianson et al., 2023; Christianson

73 and Carvalho, 2022). This process is dependent on an expanding suite of recognized E3 ligases that
74 partner with ER-localized E2 conjugases.
75
76 The ER-localized E2 enzymes Ubc6 and Ubc7 were originally identified in yeast as critical members
77 of the ERAD machinery, and the mammalian orthologs, Ube2j1/Ube2j2 and Ube2g1/Ube2g2 were
78 subsequently identified (Lenk et al. 2002; Wang et al. 2009; Abdul Rehman et al. 2024; Swarnkar et
79 al. 2024). Ubc6 and Ubc7 facilitate E3-dependent ubiquitylation by interacting with the E3s Doa10
80 and Hrd1, respectively (Kreft and Hochstrasser 2011; Zattas and Hochstrasser 2015; Lips et al. 2020;
81 Mehrtash and Hochstrasser 2022; Christianson et al. 2023). In addition, they participate in sequential
82 ubiquitylation, whereby Ubc6 first catalyzes the addition of ubiquitin to an [atypical] hydroxylated
83 amino acid (Ser or Thr) and Ubc7 then extends a ubiquitin chain via [typical] lysine modification
84 (Weber et al. 2016). Ube2j2, in particular, displays a preference for hydroxylated amino acids (Wang
85 et al. 2009; Abdul Rehman et al. 2024; Swarnkar et al. 2024), whereas Ube2j1 can utilize
86 hydroxylated residues *in vivo* (Burr et al. 2013). Also similar to yeast, Ube2j2 and Ube2g2 interact
87 with distinct ER-localized E3 ligases, including MARCH6 and HRD1, the mammalian orthologs to
88 Doa10 and Hrd1, respectively, along with RNF139 and RNF145 (reviewed in Christianson and
89 Carvalho 2022; Vrentzou et al. 2025). The conserved partnership between ERAD E2s and E3s is an
90 indicator of their central role in cellular function.
91
92 Human Ube2j1 and Ube2j2 are similar (43% amino acid sequence similarity, 27% identity), and their
93 similar (though not identical) biochemical activity suggests overlapping functions in the cell.
94 However, investigations into the activities and targets of Ube2j2 in mammalian cells highlight its
95 unique targets and physiological roles (Younger et al. 2006; van den Boomen et al. 2014; van de
96 Weijer et al. 2014; Glaeser et al. 2018; Liu et al. 2019; Cremer et al. 2021; Wolf et al. 2021; Yu et al.
97 2025). Recently, Ube2j2 has also been shown to contribute to progression and drug resistance in
98 cancer models (Kumari and Kumar 2023; Nakao et al. 2023; Lin et al. 2024). Thus, Ube2j2 plays a
99 distinct role in mammalian protein homeostasis and cell physiology.
100
101 To uncover cellular pathways associated with Ube2j2, we first used mass spectrometry to quantify
102 the proteomes of Ube2j2 CRISPR-derived knockout cells under control and tunicamycin-induced ER
103 stress conditions. We then analyzed the proteomic data using a computational network-based
104 procedure that combined the *weighted gene co-expression analysis* (WGCNA) (Langfelder and

105 Horvath, 2008) and differentially expressed proteins (DEP) (Robinson et al. 2010) approaches to
106 model changes in protein abundance and hereby provide a systems-level view of molecular
107 differences between treatments (Serin et al. 2016; Vella et al. 2017). Thus, we were able to (1) identify
108 sets of proteins (modules) with similar abundance profiles across experimental conditions, (2) define
109 module eigengenes (representative profiles that summarize the behavior of any given module,
110 calculated as the first principal component of the protein abundance data) and relate these to
111 experimental treatments, (3) annotate the modules using Gene Ontology (GO) enrichment analysis to
112 extract biological meaning (Ashburner et al. 2000), and (4) find key drivers in the different modules
113 (so-called hub genes) by identifying highly connected proteins that had strong significance in the
114 DEP analysis. To avoid confusion with the term "hub protein" (a central protein in a protein-protein
115 interaction network), we here employ the term “hub gene”, which originates from the WGCNA
116 approach, even though the present analysis is applied to protein abundance. Such hub genes provide
117 potential targets for future study into the biological processes associated with Ub2j2 expression and/or
118 ER stress.

## Results

We first used CRISPR-Cas to create a cell line of U2OS cells, C6β (denoted KO or C6 in raw data sets), lacking a region of 432 base pairs spanning the 5′ UTR and first coding exon of the *UBE2J2* gene and not displaying any visible Ube2j2 expression as probed by Immunoblotting (**Figure S1**). Then, to gain insight into changes in protein abundance as a result of ER-stress duration and the presence or absence of Ube2j2, we grew (in quadruplicate) wild-type and Ube2j2 KO cells in either dimethyl sulfoxide (DMSO; vehicle control) or 10 µg/mL tunicamycin – a cell permeable agent that prevents N-glycosylation in the ER and thereby leads to protein misfolding and activates the UPR – for 6 or 18 hours. Upon flash-freezing, the cells were then processed for and analyzed by quantitative mass spectrometry.

The resulting 32 data sets contained 5903 unique protein sequences, and the quality of samples was gauged based on the coefficient of variation of replicates, which ranged from 11.24 to 18.77% within a sample group. Samples with a coefficient of variation of 10-20% are generally considered reproducible for downstream analyses (Cho et al. 2021). The WGCNA approach defined 12 statistically separate protein abundance profiles each comprising 200-1029 proteins (**Figure 1a, Supplementary File 1**). These 12 modules were annotated to describe the expression and functional properties of the proteins within each module and their association to experimental factors. As visualized by the eigengene values for each module (**Figure 1b**), variation in protein levels across genotypes was the primary factor in defining modules, followed by tunicamycin treatment, and to a lesser extent time (**Figure 1c, Supplementary File 2**). Eigengenes represent the absolute value of changes in abundance, so the magnitude of the change, rather than the direction of change, in protein abundance is reflected in the eigengene pattern. The identified modules also had significant enrichment for specific GO categories in biological processes, cellular components and to a lesser extent molecular functions (**Supplementary File 3**), allowing additional insight into the functional properties of modules.

Four pairwise contrasts were selected to understand the effects that tunicamycin treatment has on the Ube2j2 KO cells: KO_Tu_18hr-vs-WT_Tu_18hr; KO_Crtl_18hr-vs-WT_Ctrl_18hr; KO_ Crtl _6hr-vs-KO_Ctrl_18hr; WT_ Crtl _6hr-vs-WT_ Crtl _18hr. These four comparisons were chosen for their potential to provide insight into differences in protein abundance based on changes of a single variable at a time (genotype, drug treatment, or time in culture). We chose to focus on treatment conditions at

151 18 hours, since this late timepoint was expected to provide maximal changes in protein abundance.
152 Further dissection of the modules showed that 9 out of the 12 modules were associated with at least
153 one of these selected pairwise contrasts of interest (**Figure 1d, Supplementary File 2**). Below, we
154 focus on four modules or groups of modules whose patterns of protein abundance levels support our
155 current understanding of the functions of Ube2j2 in protein homeostasis at the ER and offer new
156 insights into cellular protein networks associated with the loss of Ube2j2 and/or ER stress.

157

158 **Pink module: Response to tunicamycin is not affected by loss of Ube2j2**

159 The pink module includes proteins whose abundance is affected strongly by tunicamycin-induced
160 stress but not by cellular genotype. The eigengene for the pink module shows stable abundance over
161 time and between the wild-type and knockout cells (**Figure 1b**). However, treatment with
162 tunicamycin leads to a strong up or down regulation of these proteins, relative to the control,
163 regardless of genetic background. Proteins included in the pink module represent well-characterized
164 members of ER-stress pathways such as HERP, HSPA5 (BiP), and VIMP (SelS) (**Figure 2a-c)**, all
165 of which also showed clear upregulation in response to tunicamycin via immunoblotting (**Figure 2d)**.
166 In this manner, the pink module provides an important validation of our mass spectrometry data.
167 **Figure 2e** shows the distribution of proteins in the pink module annotated by biological process
168 ontology. These are enriched for protein processing, folding, and homeostasis as well as protein
169 synthesis and metabolism. Processes related to cytokinesis and chromosome segregation are also
170 identified in this module.

171

172 **Magenta module: Loss of Ube2j2, regardless of treatment with tunicamycin, drives changes in**
173 **protein abundance**

174 The magenta module includes 1029 proteins whose abundance is dependent on the presence or
175 absence of Ube2j2 (p-value $< 0.001$), with little-to-no additional effect of tunicamycin or time
176 (**Figure 1b**). Functional analysis of the magenta module identified significant associations with terms
177 from the cellular components and biological processes, and to a lesser extent molecular function
178 ontologies (**Supplementary File 2).** Based on this analysis, the magenta module was enriched with
179 three main categories (**Figures 3a and 3b**). First, actin-binding proteins, including some that are
180 involved with vesicular transport and exocytosis; second, regulation of mitotic cell cycle involving
181 spindle localization and segregation of sister chromatids; and third, processes that are important for
182 protein abundance regulation and homeostasis. To further narrow down the list of proteins in the

183 magenta module, we conducted a hub gene analysis and identified 135 proteins that were highly
184 connected in the magenta module and significantly associated with protein abundance differences
185 between Ube2j2 KO versus wildtype cell lines (**Figure 3c**). GO enrichment analysis of magenta hub
186 genes by cellular component (**Figure 3d**) found similar results to the module level analysis and
187 suggest that hub genes play a critical role in defining the functions associated with actin and the
188 regulation of the proteasome. Interestingly, Ube2g2, the closely related E2 enzyme that works in
189 tandem with Ube2j2 in yeast (Weber et al. 2016; Mehrtash and Hochstrasser 2022) is also included
190 in this module. This suggests that at least some of the proteins in the magenta module may directly
191 compensate for the loss of Ube2j2's enzymatic activity. Thus, at least two major cellular components
192 – actin-based motility and cellular structure, and protein degradation – are influenced by the presence
193 or absence of Ube2j2, regardless of tunicamycin-induced ER stress.
194
195 **Blue and black modules: Loss of Ube2j2 phenocopies treatment with tunicamycin**
196 The blue and black modules include proteins whose abundance in response to tunicamycin treatment
197 is phenocopied by the loss of Ube2j2 (**Figure 1b)**. Proteins that are members of the black and blue
198 modules are affiliated with a broad set of biological processes including protein-complex interactions,
199 translation initiation, and protein and RNA-localization (black module, **Figure 4a**) and vesicular and
200 ER-to-Golgi transport, electron transport, and nucleotide metabolism (blue module, **Figure 4b**).
201
202 While there are no identified hub genes for the black module, the blue module includes 20 hub genes
203 (**Figure 4c)**. Among these, a cluster of COPI coatomer proteins – COPB1, COPB2, COPG1, and
204 COPG2 – are striking due to their roles in Golgi-to-ER transport. In addition, protein homeostasis
205 components including the proteasome adapter and scaffold protein ECM29, UFM1- and SUMO-
206 activating proteins (UBA5 and SAE2, respectively), and the E3 ubiquitin ligase, listerin, are blue
207 module hub genes, along with the translation initiation factor EIF2A, which plays a central role in
208 regulating the PERK branch of the UPR (Harding et al. 2000; Hetz et al. 2015b). Thus, many blue
209 module hub genes have roles in proteostasis. Only four of the 20 hub genes for the blue module have
210 significant differences between 18 hours of tunicamycin treatment in wildtype cells and 6 hours of
211 basal conditions in mutant cells. Overall, we find that the blue and black modules describe proteins
212 whose abundance in the absence of Ube2j2 is similar to that of ER stress conditions, and for which
213 additional ER stress does not amplify the effect of the loss of Ube2j2.
214

**Purple, midnightblue, and brown modules: Effect of time in culture is abrogated in the absence of Ube2j2**

The three related modules purple, midnightblue, and brown describe a pattern wherein time-dependent changes in protein abundance under control conditions are attenuated when Ube2j2 is missing (**Figure 1b**). This could represent a change in cell-cycle progression or disparate reactions to time in culture.

In all three modules, proteins involved with ribosomal metabolism (including biogenesis and rRNA processing) are highly represented (**Figure 5**), suggesting a previously unappreciated role for Ube2j2 in ribosome biosynthesis and regulation. The GO annotations of proteins in the purple, midnightblue, and brown modules suggest that Ube2j2 may also impact protein translation during cellular growth in culture, or potentially during advancement of the cell cycle (**Figure 5**).

Only the brown module has associated hub genes and about one third of these 23 hub genes are directly associated with the ribosomal metabolism described by the annotation of the entire module. This suggests that those proteins will be strong candidates for future research into the role of Ube2j2 in regulating cellular health during culturing and growth.

## Discussion

Here, we engineered a line of U2OS cells lacking Ube2j2 and profiled their proteome alongside wild-type cells under four different conditions. Our analysis resulted in 12 modules that describe patterns of changes in protein abundance across nearly 6000 protein sequences. We identified four modules/groups of modules that are characterized by interactions between cellular genotype, treatment condition, or time in culture. GO annotation of the proteins that most strongly drive the eigengene pattern for these modules (hub genes) show that defined classes of biological functions are associated with the magenta, black and blue modules, and that three closely related modules (brown, midnightblue, and purple) show overlapping representation of the same or similar biological function.

There are, to our knowledge, two other proteomic datasets available for cells lacking wildtype Ube2j2 levels. One investigation showed that differentially downregulated proteins in Ube2j2 knockout testes cells were enriched in gamete-specific proteins-(Yu et al. 2025). The other investigation, a large-scale transcriptomic and proteomic study, found that the combined knockdown of Ube2j2 and the E1 ligase UBA1 reduced K48-linked ubiquitylation and resulted in the concomitant downregulation of Ube2D1 and Ube2E3 mRNA levels and Ube2D1 and Ube2E1 protein levels in HEK293T cells (Hunt et al. 2023). The present data set is unique because it probes the response of cells to the stress that Ube2j2 would normally help to alleviate.

Our dataset and analysis add to previously published data sets by combining the complete knockout background with a network-based perspective on changes to the proteome in response to two variables, time and drug-induced stress. Our analyses provide a suite of protein-abundance profiles that reveal both expected and unpredicted changes across the proteome in the absence of Ube2j2. Our results highlight UPR and ubiquitin-dependent protein homeostasis networks (highly represented in the pink module and magenta modules (Figures 2 and 3)). The network analysis also suggests Golgi-to-ER trafficking pathways (magenta, blue, and black modules, Figures 3 and 4) and RNA metabolism pathways (brown, purple, and midnightblue modules, Figure 5) that are dependent on Ube2j2. In addition, we were interested in any changes in abundance of the Ube2j2 paralog, Ube2j1, and the two Ubc7 homologs, Ube2g1 and Ube2g2 in this dataset. Ube2j1 and Ube2g1 are found in the brown module, which makes them members of a cohort of proteins whose reaction to time in culture is modulated by Ube2j2 (Figure 1), while Ube2g2 is a hub gene for the magenta module (Figure 3). These results suggest different types of compensation by ER-associated E2 enzymes in

264 the absence of Ube2j2. Together, the WGCNA analysis, eigengene profiles, and GO annotations that
265 accompany our data sets suggest inroads for future research by providing insights into changes in
266 protein abundance that are based entirely on the presence or absence of Ube2j2 or through complex
267 interactions between Ube2j2 and tunicamycin-induced stress and/or time in culture.

268 ## Materials and methods

269

270 **Generation of CRISPR-Cas9–Mediated UBE2J2 knockout cell line**

271 Human osteosarcoma (U2OS) cells were subjected to two rounds of CRISPR-mediated gene editing.
272 Cells were transiently co-transfected with plasmids encoding Cas9 and single guide (sg) RNAs
273 targeting UBE2J2 (sgRNA#3: 5′-CAGTAAGAGGGCTCCGACCA-3′ and sgRNA#1: 5′-
274 CCGGGTCTTTCTTAATGCGA-3′) using polyethylenimine transfection reagent. sgRNA sequences
275 were designed and kindly provided by Dr. Dick van den Boomen in the lab Prof. Paul J. Lehner,
276 University of Cambridge, UK. After 24 hours, cells were selected with 10 µg/µl Puromycin and 100
277 µg/µl Hygromycin B to enrich for transfected cells. To enhance selection efficiency and avoid false
278 positives, cells were split three days post-transfection. Selection medium was replaced once non-
279 transfected controls were eliminated. Due to variable sgRNA efficiency and to obtain a homogenous
280 population of cells, single-cell clones were isolated by limiting dilution (0.3 cells/well in 96-well
281 plates), expanded, and harvested.

282

283 Genomic DNA was extracted from potential knockout clones using QuickExtract™ DNA Extraction
284 Solution 1.0 (Epicentre), following the manufacturer's instructions. Briefly, ~9,000 cells were
285 pelleted at 500 × g for 5 min, washed in phosphate buffered saline (PBS), and resuspended in 50 µL
286 QuickExtract™. Extracts were incubated at 70°C for 30 minutes with intermittent vortexing, followed
287 by 95°C for 5 min.

288

289 The extracted genomic DNA was used as template for PCR amplification prior to TOPO cloning and
290 Sanger sequencing. PCR reactions were performed using the Phusion DNA polymerase (Thermo
291 Fisher Scientific) with a primer pair designed to amplify a region of the gene covering the sgRNA
292 target site (FWD: 5′-GGCCAGGGCATAAGAGTTTATTTAC-3′, REV: 5′-
293 TACTGCTCTGTCGAAACACTGC-3′), yielding an expected amplicon size of 1472 bp. PCR
294 products were verified by agarose gel electrophoresis and subsequently ligated into the pCR™-Blunt
295 II-TOPO™ vector using the Zero Blunt™ TOPO™ PCR Cloning Kit (Thermo Fisher Scientific),
296 following the manufacturer's protocol. The ligation products were transformed into competent *E. coli*
297 DH5α cells, and ten colonies per reaction were picked for overnight culture. Plasmid DNA was
298 isolated using mini-prep procedures and subjected to Sanger sequencing (Eurofins) using the M13

299 reverse -29 primer (5′-CAGGAAACAGCTATGACC-3′). Sequencing analysis revealed a 432 bp
300 deletion in the targeted *UBE2J2* locus (**Supplementary Figure 1**).
301
302 **Generation of a monoclonal anti-VIMP antibody**
303 Mouse monoclonal antibodies were raised to human VIMP using a previously described protocol
304 (Hendil 2005). For immunization, we used the $His_6$-lipoFF-tagged cytosolic region (residues 49–189)
305 of human VIMP with the Sec residue at position 188 replaced with a Cys residue. The protein was
306 produced recombinantly as previously described (Christensen et al. 2012).
307
308 **Cell culture, tunicamycin treatment, and harvest**
309 Wild-type or knock-out U2OS cells were grown maintained in Dulbecco's Modified Eagles Medium
310 supplemented with L-glutamine and heat-treated fetal bovine serum. Cells were passaged regularly,
311 and experiments were performed with cells that had been passaged fewer than 20 times. For drug
312 treatment experiments prior to immunoblotting, cells were treated by adding 10 µg/mL tunicamycin
313 (final concentration) directly to growth media followed by incubation for the indicated times. As a
314 control, 0.01% DMSO (vehicle control, final concentration) was added to cells, which were then
315 incubated for the longest incubation time.
316
317 **Protein concentration determination, SDS-PAGE, and immunoblotting**
318 Cells were harvested by placing plates on ice and washing with PBS, followed by lysis on ice in 40
319 uL radioimmunoprecipitation assay (RIPA) buffer supplemented with phenylmethylsulfonyl fluoride
320 (0.01%) and cOmpleteMini protease inhibitor mixture (1 tablet per 10 mL of buffer, according to
321 manufacturer's directions). Cells were scraped off from the plates and sonicated for five seconds on
322 ice. Cell lysates were centrifuged for 7.5 minutes at 12,500 rpm at 4°C and supernatant was removed
323 to fresh tubes for analysis. Protein content of cleared lysates was determined by quantitative
324 Bicinchoninic Acid (BCA, Sigma Aldrich) anlysis in 96-well plate format using bovine serum
325 albumin (Sigma Aldrich) as standard. All dilutions for the standard curve and sample measurements
326 were done in triplicates. The BCA was measured at 562 nm using a plate reader (Tecan) and
327 equivalent portions of lysate were run on acrylamide gels and transferred to polyvinylidene fluoride
328 for immunoblotting. Immunostaining was performed with the following primary antibodies, which
329 were diluted in Tris buffered saline plus 0.05% Tween containing 5% non-fat milk or bovine serum
330 albumin: rabbit anti-BiP/GRP78 (Sigma, GL-19; RRID:AB_477030) (1:1000), rabbit anti-HERP

331 (kind gift from L. Hendershot) (1:1000), rabbit anti-Ube2j2 (kind gift from L. Hendershot) (1:1000),
332 mouse anti-VIMP (described above) (1:1000). Primary antibodies were detected with secondary
333 antibodies conjugated to Horseradish Peroxidase (Pierce) diluted 1:100,000 in Tris buffered saline
334 plus 0.05% Tween containing 5% non-fat milk. Blots were visualized using Pierce Femto ECL
335 according to manufacturer's directions.
336
337 **Cell treatment, growth and harvest for mass spectrometry**
338 Wild-type or knockout cells were grown to approximately 50% confluency in 10 cm plates. Cells
339 were grown as described above and then treated by replacing original growth media with media
340 supplemented with 0.01% DMSO (vehicle control) or 10 µg/mL tunicamycin in DMSO followed by
341 incubation for 6 or 18 hours. Media was removed by aspiration and plates were moved onto ice. Cells
342 were scraped off plates into PBS supplemented with protease inhibitor (cOmpleteMini protease
343 inhibitor mixture was dissolved in PBS according to manufacturer's direction). Cells were spun
344 gently (5 min at 2000 rpm, at 4°C) and washed twice with ice cold PBS supplemented with protease
345 inhibitors. Cell pellets were snap frozen in liquid nitrogen and stored at -80°C.
346
347 **Mass spectrometry procedure**
348 In preparation for mass spectrometry, cell pellets were lysed in lysis buffer (1% sodium deoxycholate,
349 100 mM Tris-HCl, pH 8.5) and incubated for 10 min at 99°C, followed by sonication in a Bioruptor
350 Pico (20 cycles, 30 s on/30 s off, ultra-low frequency). Lysates were cleared by centrifugation,
351 reduced with 5 mM TCEP for 15 min at 55°C, and alkylated with 20 mM chloroacetamide for 30 min
352 at room temperature. Proteins were digested for 16 h at 37°C using trypsin and LysC at a 1:100
353 (enzyme:protein) ratio. Peptides were acidified with 1% trifluoroacetic acid and desalted using SDB-
354 RPS StageTips.
355
356 Peptides were separated on a 50 cm × 75 µm ID home-packed analytical column containing ReproSil-
357 Pur C18-AQ resin (1.9 µm; Dr. Maisch) using an EASY-nLC 1200 ultra-high-pressure system.
358 Samples were loaded in buffer A (0.1% formic acid) and separated using a non-linear gradient from
359 5% to 60% buffer B (0.1% formic acid, 80% acetonitrile) over 50 min at a flow rate of 300 nL/min.
360 Peptides were introduced via a CaptiveSpray source with a 10 µm emitter into a timsTOF Pro2 mass
361 spectrometer (Bruker) operated in diaPASEF mode.

362 MS data were acquired over a 100–1700 m/z range using the standard long-gradient diaPASEF
363 method, comprising 16 diaPASEF scans with two 25 Da windows per ramp, covering a total mass
364 range of 400–1201 Da and an ion mobility range of 1.43–0.6 $1/K_0$. Collision energy decreased linearly
365 from 59 eV at $1/K_0 = 1.6$ to 20 eV at $1/K_0 = 0.6$ Vs $cm^{-2}$. Both accumulation and PASEF ramp times
366 were set to 100 ms, resulting in a total cycle time of 1.17 s.
367
368 Quantification of raw data was performed using Spectronaut v15.5 (Bruderer et al. 2015) in directDIA
369 mode using the *Homo sapiens* UniprotKB FASTA (UP000005640; TaxID 9606).
370 Carbamidomethylation of cysteine was set as a fixed modification; oxidation of methionine and
371 protein N-terminal acetylation were set as variable modifications. Up to two missed cleavages were
372 allowed, and a minimum peptide length of seven amino acids was required. The false discovery rate
373 (FDR) at the PSM, peptide, and protein group level was set to 0.01. The raw data processing was
374 implemented in the automated analysis pipeline of the Clinical Knowledge Graph (Santos et al. 2022)
375 and exported as label-free quantitative (LFQ) intensities. The LFQ intensities were normalized by
376 log2 transformation and proteins with less than at least 2 valid values in at least one group were
377 filtered out. Missing values were imputed using the MinProb approach (width=0.2 and shift=1.8,
378 (Lazar et al. 2016)) and with Mixed imputation.
379
380 **Bioinformatics analysis**
381 The quantifications from 5903 proteins were used to identify differentially expressed proteins and
382 generate weighted gene co-expression network analysis.

383 The differential expression analysis was done using edgeR (v3.40.2; (Chen et al. 2025) and the protein
384 intensities were normalized with the trimmed mean of M-values method. Generalized linear models
385 were used to determine if differences in protein intensities were associated with the main effects from
386 the experimental design: genotypes (wildtype and Ube2j2 KO) and cell treatments (vehicle control
387 and tunicamycin) at 6 or 18 hours. Pairwise contrasts for DEPs were specified using the emmeans
388 package (v1.8.7; Lenth and Piaskowski 2017) in R and focused on the effect of tunicamycin treatment
389 has on Ube2j2 mutants through time (KO_Tu_18hr-vs-WT_Tu_18hr; KO_Ctrl_18hr-vs-
390 WT_Ctrl_18hr ; KO_Ctrl_6hr-vs-KO_Ctrl_18hr; WT_Ctrl_6hr-vs-WT_Ctrl_18hr). To determine if
391 a protein was significantly differential expressed with main experiential factors or pairwise contrasts
392 a Benjamini-Hochberg adjusted p-value was less than 0.05. DEPs with significant pairwise contrasts
393 were also used as a criterion for hub gene analysis.

394 Co-expression analysis and module identification were conducted using functions from WGCNA
395 (v1.72-1; (Langfelder et al. 2008). The soft threshold was determined as the value producing a >90%
396 model fit to the scale-free topology and low mean connectivity. Co-expression relationships were
397 calculated using unsigned Pearson's correlation coefficients raised to the soft threshold and grouped
398 using hierarchical clustering of dissimilarity among the unsigned topological overlap matrix. Modules
399 were identified using dynamicTreeCut (v1.62-1; (Langfelder et al. 2008)) with parameters of
400 minimum module size of 100, deep split value of 2, and cut height of 0.99. Module eigengenes were
401 calculated as the first principal component of the expression matrix and modules with correlated
402 (>0.80) eigengene values were collapsed because these modules contained proteins that strongly
403 covary in abundance across samples.
404
405 The biological meaning of the co-expression modules was investigated using three approaches. First,
406 we tested if module eigengenes were associated with the main effects of the experimental conditions
407 using generalized linear models. Specifically, we tested if module eigengenes were significantly
408 associated with differences between genotypes (wildtype and Ube2j2 KO) or cell treatments (vehicle
409 control and tunicamycin) at 6 or 18 hours. Second, functional annotation of the modules as conducted
410 using gene ontology (GO) enrichment analysis. GO enrichment for each ontology (biological rocess,
411 molecular function, or cellular component) was performed using the clusterProfiler package (v4.17.0;
412 (Yu et al. 2012) and bioconductor Human annotation database (org.Hs.eg.db; v3.18). Visualization
413 of GO enrichment results were done using enrichplot (v1.29.1) and simplifyEnrichment (v1.6.1; (Gu
414 and Hübschmann, 2023). GO terms were determined to be significant if the Benjamini-Hochberg
415 adjusted p-value was less than 0.05. Third, hub genes within modules were identified by examining
416 the interaction between module membership and the –log10 p-values for at least one of the specific
417 pairwise contrasts. Module membership was calculated as the absolute of the Pearson's correlation
418 between the module eigengene and protein LFQ intensities. The threshold for module membership
419 was having a greater than 0.85 correlation, and the DEP threshold was a –log10 adjusted p-value of
420 greater than 2.
421
422 **Data availability**
423 Cell lines are available upon request. Please refer to the Reagent Table for futher details about cell
424 lines and antibodies. Supplemental files available at FigShare. Supplementary File 1 contains the
425 module assignments and accession numbers for proteins in the dataset. Supplementary File 2 contains

426 the raw and adjusted pvalues used to generate Figure 1C & 1D in this manuscript. Supplementary
427 File 3 contains the GO annotations for proteins in each module. Code generated for the analyses
428 described can be found at: https://github.com/mzinkgraf/Ube2j2 . The mass spectrometry proteomics
429 data have been deposited to the ProteomeXchange Consortium via the PRIDE partner repository
430 (Perez-Riverol et al. 2025) with the dataset identifier PXD076153.
431
432
433 **Acknowledgements**
434 We acknowledge Dick J. H. van den Boomen (Cambridge Institute for Medical Research, University
435 of Cambridge, UK) for the design of sgRNA sequences and Linda M. Hendershot (St. Jude Children's
436 Research Hospital, Memphis, USA) for kindly providing us with rabbit anti-HERP and rabbit anti-
437 Ube2j2 antibodies.
438
439 **Funding**
440 Mass spectrometry-based proteomics analyses were performed by the Proteomics Research
441 Infrastructure (PRI) at the University of Copenhagen (UCPH), supported by the Novo Nordisk
442 Foundation (NNF) (grant agreement number NNF19SA0059305). CLD was supported by funding
443 from the American Scandinavian Foundation and the Fulbright U.S. Scholar Program. Support for
444 this research was also provided by the Lizzi og Mogens Staal Fond (grant number 2024-1314). LE
445 was supported by the Department of Biology, University of Copenhagen, and a sabbatical grant from
446 the Lundbeck Foundation (grant number R500-2024-1904).
447
448 **Conflict of interest**
449 The authors declare no conflicts of interest.
450
451 **Author contributions**
452 Conceptualization, C.L.D. and L.E.; Data curation, C.L.D. and M.Z.; Formal Analysis, M.Z.; Funding
453 acquisition, C.L.D. and L.E.; Investigation, C.L.D., S.H.L., C.L.S., Q.G., E.B., R.H.P. ; Project
454 administration, C.L.D. and L.E.; Supervision, L.E.; Visualization, C.L.D., M.Z., and S.H.L.;
455 writing—original draft preparation, C.L.D., M.Z., and L.E.; writing—review and editing, all authors.
456 All authors have read and agreed to the published version of the manuscript.
457

458 **Abbreviations**

459 DEP, differentially expressed protein; DMSO, dimethyl sulfoxide; DUB, deubiquitylating enzyme;
460 ER, endoplasmic reticulum; ERAD, ER-associated degradation; GO, gene ontology; KO, knockout;
461 LB, lysogeny broth; LFQ, label-free quantitative; MS, mass spectrometry; PBS, phosphate buffered
462 saline; SDS-PAGE, sodium dodecyl sulfate-polyacrylamide gel electrophoresis; UPR, unfolded
463 protein response.; WGCNA, weighted gene co-expression analysis; WT, wildtype.

464

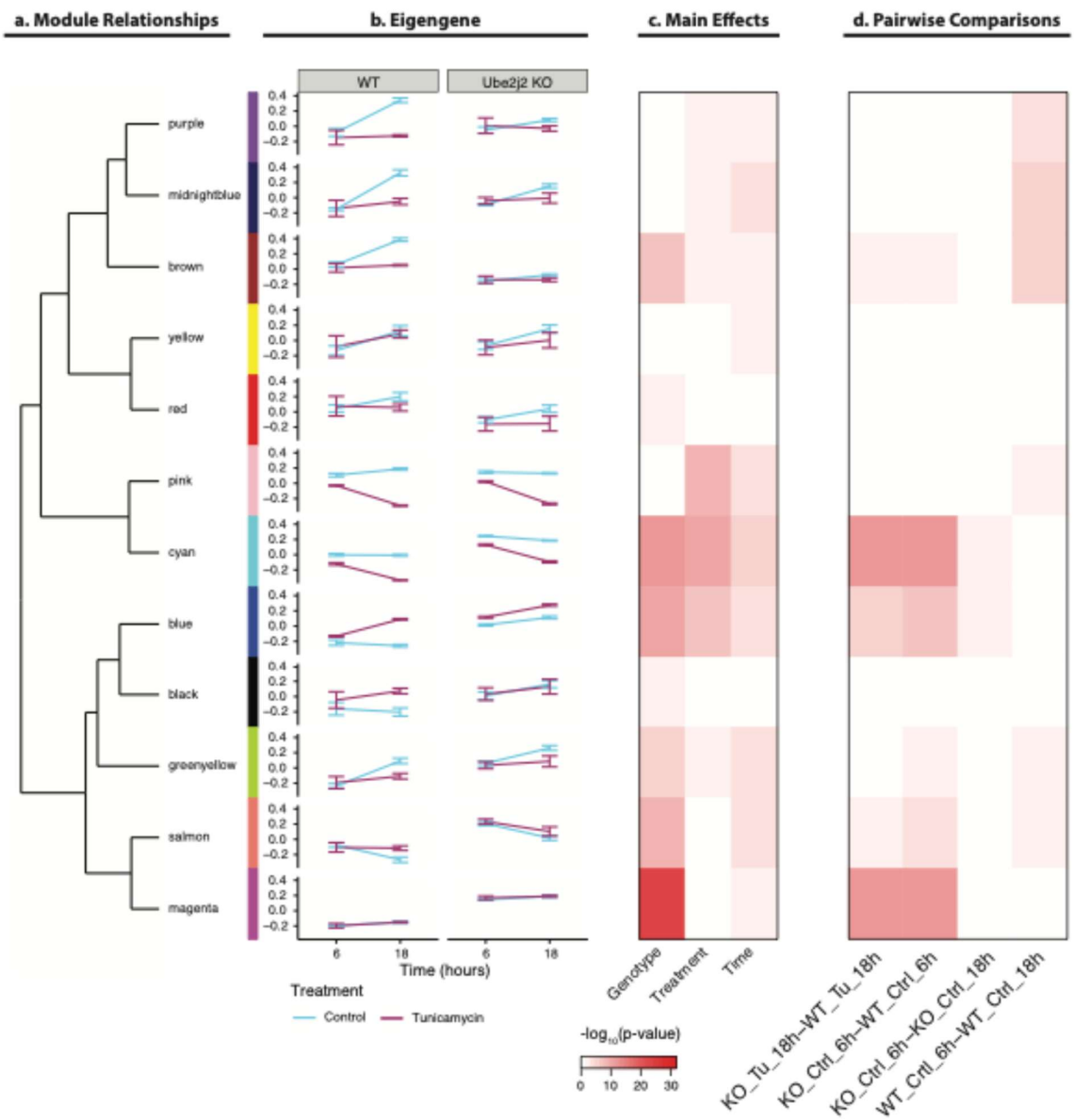


465

466 **Figure 1. Overview of proteomic data gathered from WT and Ube2j2 knockout (KO) cells in**
467 **four conditions.**

468 (**a**) Dendrogram showing the relatedness of eigengenes between modules (named by color). (**b**) Line
469 graphs of eigengene expression from the wildtype (WT) and Ube2j2 mutant (KO) genotypes across
470 treatment (control and tunicamycin) and time (6 and 18 hours). (**c**) Heatmap of –log10 p-value of
471 module eigengene significance for main effects from an ANOVA model. (**d**) Heatmap of –log10 p-

472 value of the comparisons of interest for each of the modules. The smaller the p-value (the warmer the
473 color), the more significant the difference between conditions.
474

475 ALT TEXT: Graphical figure with panels labeled a through d. The figure includes a
476 dendrogram that shows the relationship between different protein abundance modules
477 (named by colors). The eigen gene that describes the changes in protein abundance in
478 wildtype and Ube2j2 cells lines is shown next to each module. Two heat maps show the
479 statistical relevance of different conditions and pairwise comparisons between conditions
480 for each module with darker colors representing lower p-values.

481
482

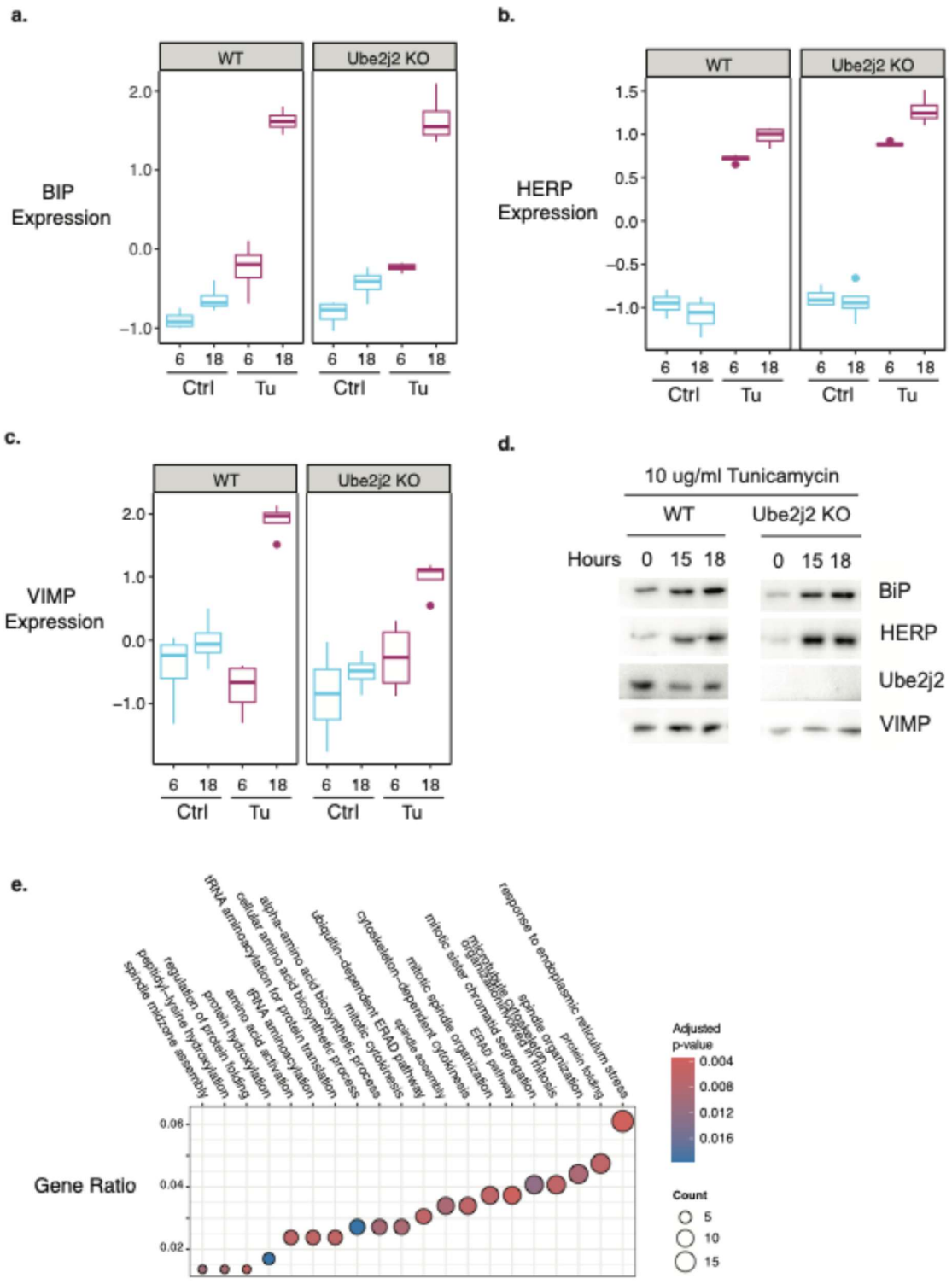


483

484 **Figure 2. Quantitative relative expression data and immunoblot validation for individual**
485 **proteins in the pink module.** Graphs show changes in protein abundance for (**a**) BiP, (**b**) HERP, and

486 (**c**) VIMP in wildtype and Ube2j2 deletion cells in each of the four conditions (DMSO control at 6
487 and 18 hours, or tunicamycin treatment at 6 and 18 hours). (**d**) Representative immunoblot of U2OS
488 cells following treatment with tunicamycin for the indicated times. Cell lysates were normalized by
489 a BCA assay prior to SDS-PAGE loading, and blots were probed for the three UPR-associated
490 proteins and Ube2j2. (**e**) GO enrichment analysis of proteins present in the pink module using the
491 biological processes ontology. The graph shows the top 20 most significant terms (adjusted p-value
492 of <0.05) and the count of module proteins observed in each term.
493

494 ALT TEXT: Three box-and-whisker plots labeled a through c show how the abundance of
495 three individual proteins change in wildtype and Ube2j2 knockout cells under different
496 conditions. An immunoblot labeled d shows corresponding biochemical data for the
497 same three proteins.

498

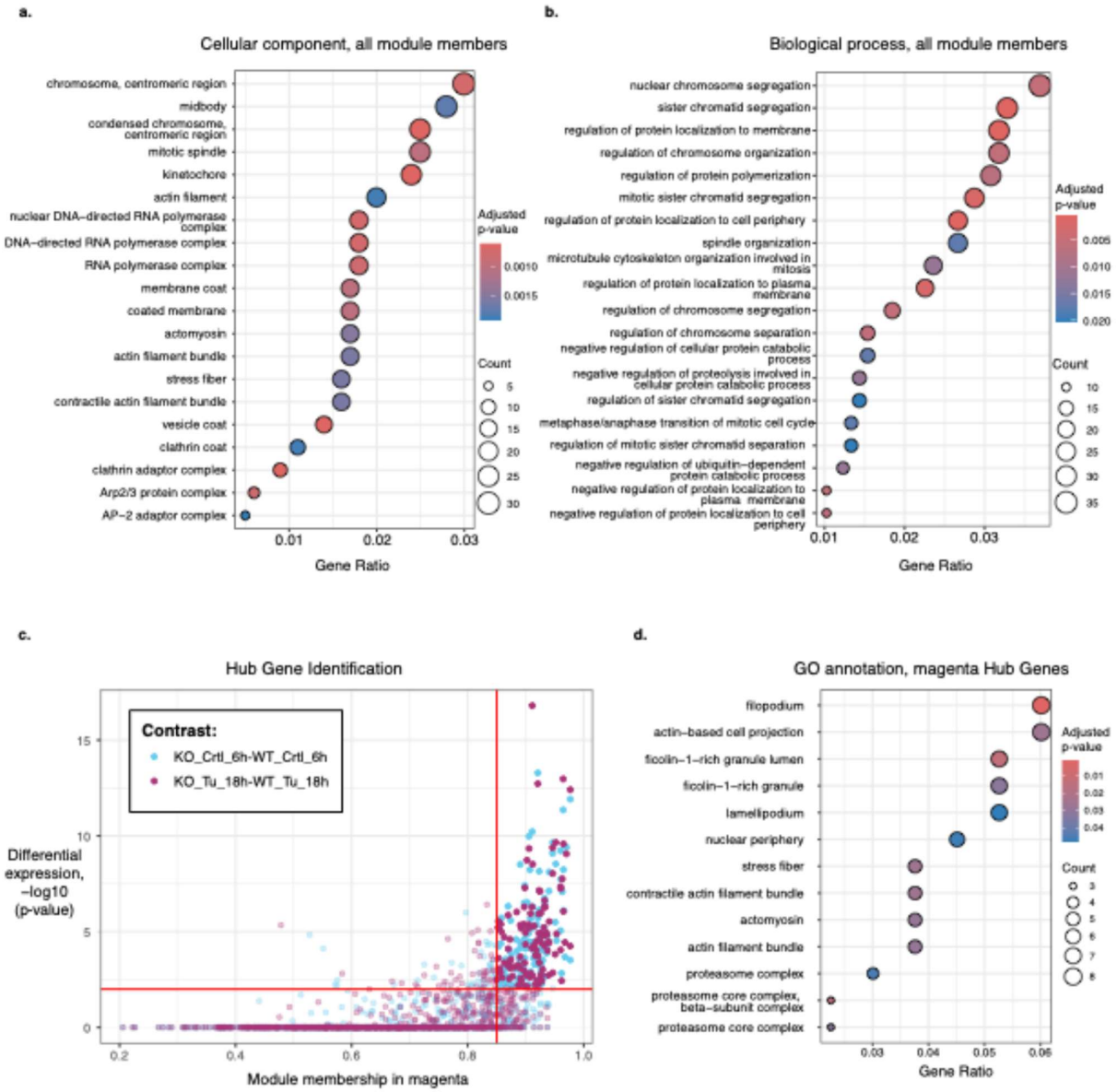


**Figure 3. Functional annotation and hub gene analysis for the magenta module.** GO enrichment analysis of all protein in the magenta module using the (**a**) cellular component and (**b**) biological processes ontology. The graphs show the most significant terms (adjusted p-value of <0.05) and the count of module proteins observed in each term. (**c**) Hub genes (upper right quadrant) in the magenta module were identified as genes having both a module membership greater then 0.85 and significant (adjusted p-value <0.05) differential abundance with at least one of the pairwise comparisons that relate to changes in protein abundance between KO vs WT cells over time. Proteins that are in the magenta module but are not hub genes are displayed in muted colors in the remaining three quadrants

508 of the graph. (**d**) GO enrichment analysis of all proteins present in the magenta module using the
509 cellular component ontology. The graph shows the top 20 most significant terms (adjusted p-value of
510 <0.05) and the count of module proteins observed in each term.
511
512 ALT TEXT: Three graphs (a, b, d) show the distribution of GO annotations across proteins
513 and hub genes in the magenta module. Circles representing the number of proteins with
514 any given GO annotation are colored according to their statistical significance, with red
515 and blue representing higher and low statistical significance, respectively. Graph c is
516 divided into quadrants. The upper right quadrant includes subset of hub genes in the
517 magenta module accumulate differently depending on their exposure to tunicamycin in
518 Ube2j2 cells.

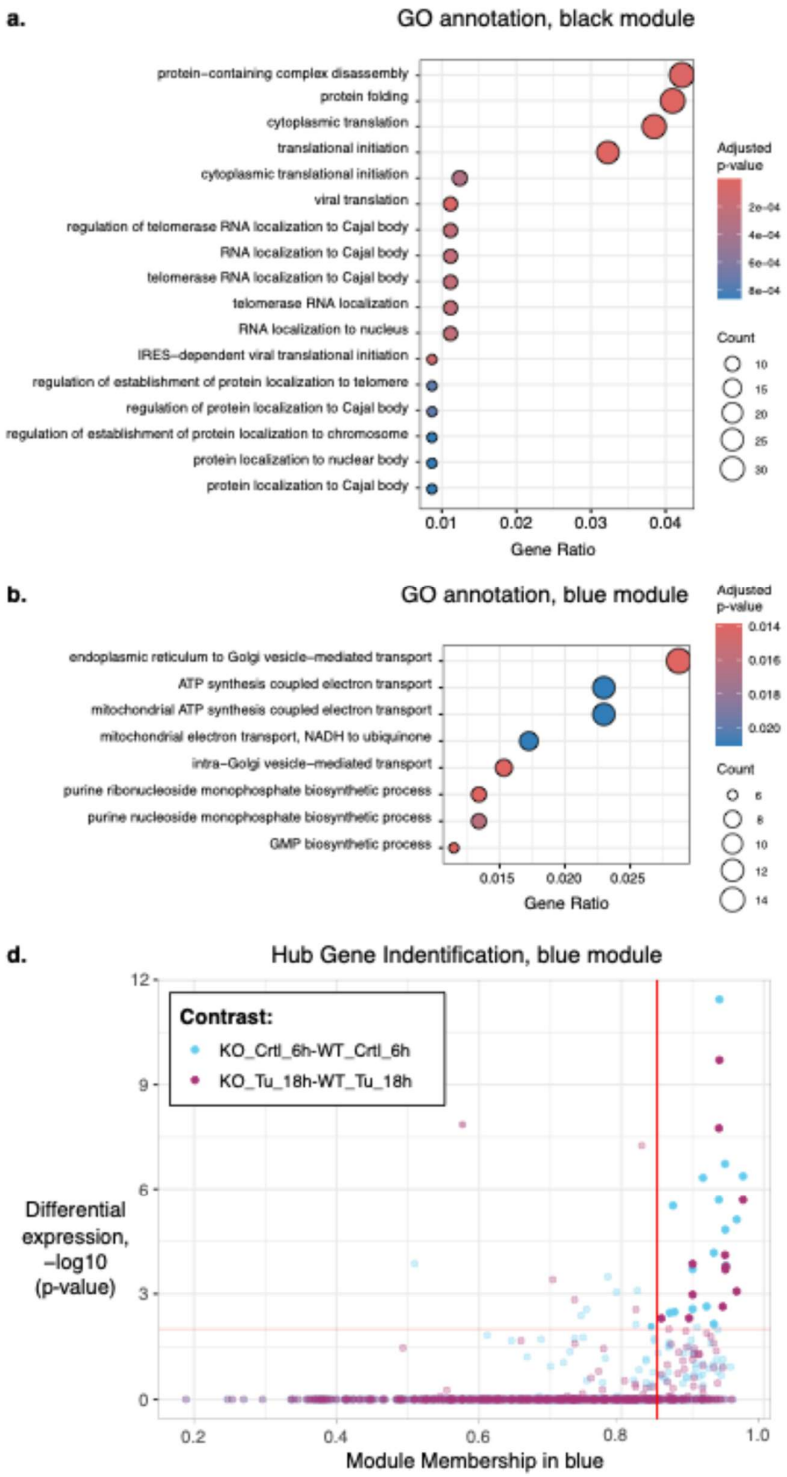


**Figure 4. Analysis of the black and blue modules.** **(a)** GO enrichment of proteins present in the black module using the biological process **(b)** GO enrichment of proteins present in the blue module using the biological process. Graphs show the top significant (adjusted p-value < 0.05) terms and the

523 count of module proteins observed in each term. (**c**) Identification of hub genes (upper right quadrant)
524 in the blue module showing proteins with high module membership (>0.85) and significant
525 association with at least one pairwise comparison that relate to changes in protein abundance between
526 KO vs WT cells over time.
527
528 ALT TEXT: Two graphs (a, b) show the distribution of GO annotations across proteins and
529 hub genes in the black and blue modules, respectively. Circles representing the number of
530 proteins with any given GO annotation are colored according to their statistical
531 significance, with red and blue representing higher and low statistical significance,
532 respectively. Graph c is divided into quadrants. The upper right quadrant includes subset
533 of hub genes in the blue module accumulate differently depending on their exposure to
534 tunicamycin in Ube2j2 cells.

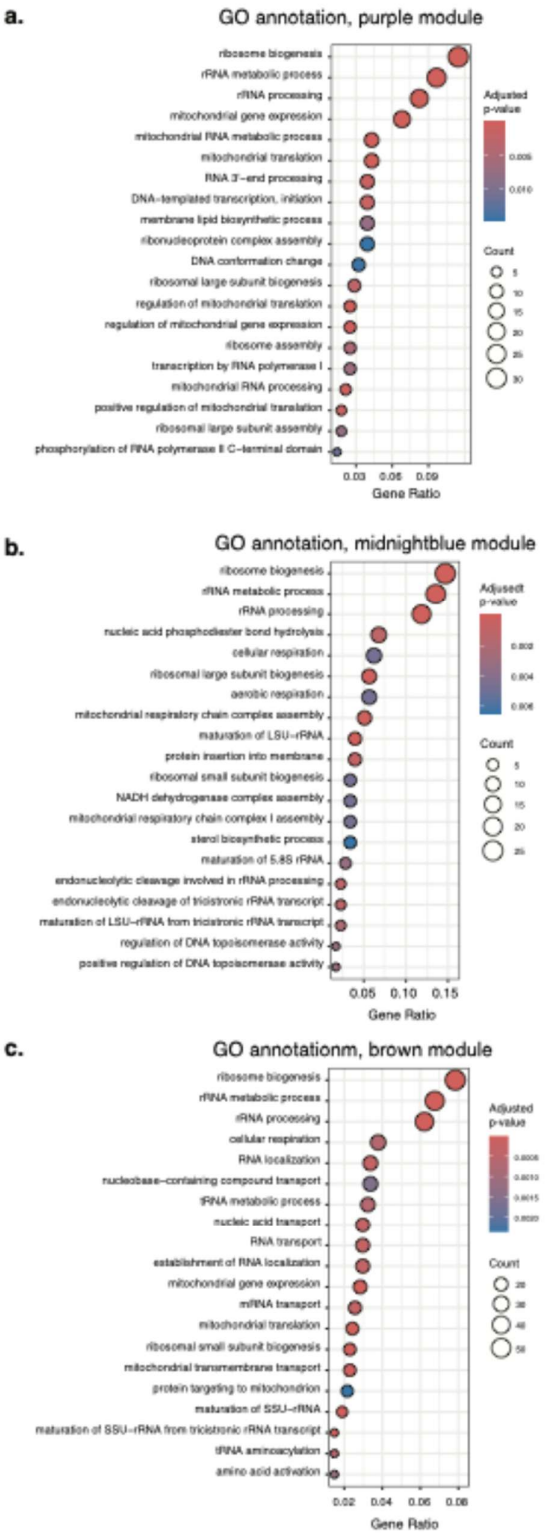


535

536 **Figure 5.** GO enrichment analysis of proteins present in the (**a**) purple, (**b**) midnightblue, and (**c**)

537 brown modules using the biological process ontology. Terms are significant with an adjusted p-value
538 of <0.05.
539

540 ALT TEXT: Three graphs labeled a, b, and c show the distribution of GO annotations
541 across proteins and hub genes in the purple, midnightblue, and brown modules. Circles
542 representing the number of proteins with any given GO annotation are colored according
543 to their statistical significance, with red and blue representing higher and low statistical
544 significance, respectively.

545
546

547

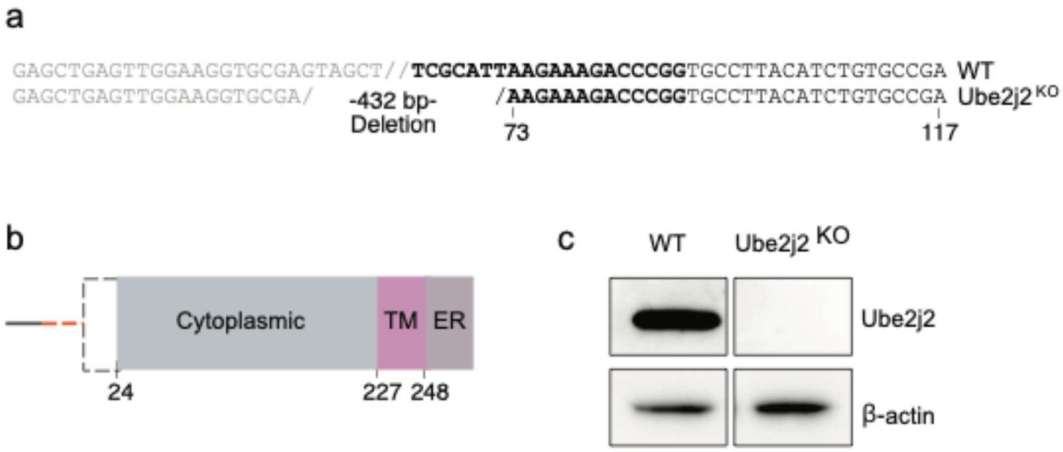


548

549

550 **Supplementary Figure 1. Generation and verification of Ube2j2 KO cell line.** (**a**) Nucleotide
551 sequence of the mutated *UBE2J2* clone, illustrating a 432 bp deletion that spans both non-coding
552 (grey) and coding (black) regions. Base numbering is relative to the start of exon 2, the first coding
553 exon. (**b**) Schematic representation of the Ube2j2 protein domain architecture. The deleted region is
554 indicated by black dashed lines in the protein and by an orange dashed line in the upstream nucleic
555 acid sequence. Numbers refer to amino acid residues; TM: transmembrane domain; ER:
556 endoplasmic reticulum lumen localization. (**c**) Immunoblot analysis of protein lysates from wild-
557 type (WT) and *UBE2J2* knockout (KO) U2OS cells. β-actin serves as a loading control.

558

559

560 ALT TEXT: A figure with three panels labeled a, b and c. a and c show the DNA
561 sequence and schematic representations of the Ube2j2 knock-out in the cells used in this
562 study. c shows the immunoblot that confirmed the successful removal of the Ube2j2
563 protein in the cells used in this study.

564

565 **References**


566 Abdul Rehman SA et al. 2024. Discovery and characterization of noncanonical E2-conjugating
567 enzymes. Science Advances. 10(13):eadh0123 [accessed 2025 Oct 5].
568 https://www.science.org/doi/10.1126/sciadv.adh0123. https://doi.org/10.1126/sciadv.adh0123

569 Ashburner M et al. 2000. Gene Ontology: tool for the unification of biology. Nat Genet. 25(1):25–
570 29 [accessed 2025 Oct 31]. https://www.nature.com/articles/ng0500_25.
571 https://doi.org/10.1038/75556

572 van den Boomen DJH et al. 2014. TMEM129 is a Derlin-1 associated ERAD E3 ligase essential for
573 virus-induced degradation of MHC-I. Proceedings of the National Academy of Sciences.
574 111(31):11425–11430 [accessed 2025 Oct 5].
575 https://www.pnas.org/doi/full/10.1073/pnas.1409099111. https://doi.org/10.1073/pnas.1409099111

576 Bruderer R et al. 2015. Extending the Limits of Quantitative Proteome Profiling with Data-
577 Independent Acquisition and Application to Acetaminophen-Treated Three-Dimensional Liver
578 Microtissues *[S]. Molecular & Cellular Proteomics. 14(5):1400–1410 [accessed 2025 Oct 5].
579 https://www.mcponline.org/article/S1535-9476(20)32885-1/abstract.
580 https://doi.org/10.1074/mcp.M114.044305

581 Burr ML et al. 2013. MHC class I molecules are preferentially ubiquitinated on endoplasmic
582 reticulum luminal residues during HRD1 ubiquitin E3 ligase-mediated dislocation. Proceedings of
583 the National Academy of Sciences. 110(35):14290–14295 [accessed 2025 Oct 5].
584 https://www.pnas.org/doi/full/10.1073/pnas.1303380110. https://doi.org/10.1073/pnas.1303380110

585 Carvalho P, Goder V, Rapoport TA. 2006. Distinct Ubiquitin-Ligase Complexes Define Convergent
586 Pathways for the Degradation of ER Proteins. Cell. 126(2):361–373 [accessed 2025 Oct 5].
587 https://www.cell.com/cell/abstract/S0092-8674(06)00857-9.
588 https://doi.org/10.1016/j.cell.2006.05.043

589 Chen Y et al. 2025. edgeR v4: powerful differential analysis of sequencing data with expanded
590 functionality and improved support for small counts and larger datasets. Nucleic Acids Research.
591 53(2):gkaf018 [accessed 2025 Oct 5].
592 https://academic.oup.com/nar/article/doi/10.1093/nar/gkaf018/7973897.
593 https://doi.org/10.1093/nar/gkaf018

594 Cho K-C et al. 2021. Evaluation of the sensitivity and reproducibility of targeted proteomic analysis
595 using data independent acquisition for serum and cerebrospinal fluid proteins. J Proteome Res.
596 20(9):4284–4291 [accessed 2025 Oct 31]. https://pmc.ncbi.nlm.nih.gov/articles/PMC8631582/.
597 https://doi.org/10.1021/acs.jproteome.1c00238

598 Christensen LC et al. 2012. The human selenoprotein VCP-interacting membrane protein (VIMP) is
599 non-globular and harbors a reductase function in an intrinsically disordered region. J Biol Chem.
600 287(31):26388–26399. https://doi.org/10.1074/jbc.M112.346775

601 Christianson JC, Carvalho P. 2022. Order through destruction: how ER-associated protein
602 degradation contributes to organelle homeostasis. The EMBO Journal. 41(6):e109845 [accessed
603 2024 Feb 19]. https://www.embopress.org/doi/full/10.15252/embj.2021109845.
604 https://doi.org/10.15252/embj.2021109845

605 Christianson JC, Jarosch E, Sommer T. 2023. Mechanisms of substrate processing during ER-
606 associated protein degradation. Nat Rev Mol Cell Biol. 24(11):777–796.
607 https://doi.org/10.1038/s41580-023-00633-8

608 Cremer T et al. 2021. The ER-embedded UBE2J1/RNF26 ubiquitylation complex exerts
609 spatiotemporal control over the endolysosomal pathway. Cell Reports. 34(3):108659 [accessed
610 2025 Oct 5]. https://linkinghub.elsevier.com/retrieve/pii/S221112472031648X.
611 https://doi.org/10.1016/j.celrep.2020.108659

612 Fischer JA. 2003. Deubiquitinating enzymes: their roles in development, differentiation, and
613 disease. Int Rev Cytol. 229:43–72 [accessed 2012 Mar 15].
614 http://www.ncbi.nlm.nih.gov/pubmed/14669954

615 Glaeser K et al. 2018. ERAD-dependent control of the Wnt secretory factor Evi. The EMBO
616 Journal. 37(4):e97311 [accessed 2025 Oct 5].
617 https://www.embopress.org/doi/10.15252/embj.201797311.
618 https://doi.org/10.15252/embj.201797311

619 Gu Z, Hübschmann D. 2023. *SimplifyEnrichment* : A Bioconductor Package for Clustering and
620 Visualizing Functional Enrichment Results. Genomics, Proteomics & Bioinformatics. 21(1):190–
621 202 [accessed 2025 Oct 31]. https://academic.oup.com/gpb/article/21/1/190/7274174.
622 https://doi.org/10.1016/j.gpb.2022.04.008

623 Gundogdu M, Walden H. 2019. Structural basis of generic versus specific E2–RING E3 interactions
624 in protein ubiquitination. Protein Science. 28(10):1758–1770 [accessed 2025 Oct 5].
625 https://onlinelibrary.wiley.com/doi/10.1002/pro.3690. https://doi.org/10.1002/pro.3690

626 Harding HP et al. 2000. Regulated translation initiation controls stress-induced gene expression in
627 mammalian cells. Mol Cell. 6(5):1099–1108. https://doi.org/10.1016/s1097-2765(00)00108-8

628 Hendil KB. 2005. Development and use of antiproteasome monoclonal antibodies. Methods
629 Enzymol. 398:439–453. https://doi.org/10.1016/S0076-6879(05)98036-1

630 Hetz C, Chevet E, Oakes SA. 2015a. Proteostasis control by the unfolded protein response. Nat Cell
631 Biol. 17(7):829–838 [accessed 2025 Oct 2]. https://www.nature.com/articles/ncb3184.
632 https://doi.org/10.1038/ncb3184

633 Hetz C, Chevet E, Oakes SA. 2015b. Proteostasis control by the unfolded protein response. Nat Cell
634 Biol. 17(7):829–838. https://doi.org/10.1038/ncb3184

635 Hunt LC et al. 2023. An adaptive stress response that confers cellular resilience to decreased
636 ubiquitination. Nat Commun. 14(1):7348 [accessed 2025 Oct 5].
637 https://www.nature.com/articles/s41467-023-43262-7. https://doi.org/10.1038/s41467-023-43262-7

638 Kreft SG, Hochstrasser M. 2011. An unusual transmembrane helix in the endoplasmic reticulum
639 ubiquitin ligase Doa10 modulates degradation of its cognate E2 enzyme. J Biol Chem.
640 286(23):20163–20174. https://doi.org/10.1074/jbc.M110.196360

641 Kumari S, Kumar P. 2023. Identification and characterization of putative biomarkers and
642 therapeutic axis in Glioblastoma multiforme microenvironment. Front Cell Dev Biol. 11 [accessed

643 2025 Oct 5]. https://www.frontiersin.org/journals/cell-and-developmental-
644 biology/articles/10.3389/fcell.2023.1236271/full. https://doi.org/10.3389/fcell.2023.1236271

645 Langfelder P, Zhang B, Horvath S. 2008. Defining clusters from a hierarchical cluster tree: the
646 Dynamic Tree Cut package for R. Bioinformatics. 24(5):719–720 [accessed 2025 Oct 5].
647 https://academic.oup.com/bioinformatics/article/24/5/719/200751.
648 https://doi.org/10.1093/bioinformatics/btm563

649 Lazar C et al. 2016. Accounting for the Multiple Natures of Missing Values in Label-Free
650 Quantitative Proteomics Data Sets to Compare Imputation Strategies. J Proteome Res. 15(4):1116–
651 1125 [accessed 2025 Oct 5]. https://pubs.acs.org/doi/10.1021/acs.jproteome.5b00981.
652 https://doi.org/10.1021/acs.jproteome.5b00981

653 Lenk U et al. 2002. A role for mammalian Ubc6 homologues in ER-associated protein degradation.
654 Journal of Cell Science. 115(14):3007–3014 [accessed 2025 Oct 5].
655 https://doi.org/10.1242/jcs.115.14.3007. https://doi.org/10.1242/jcs.115.14.3007

656 Lenth RV, Piaskowski J. 2017. emmeans: Estimated Marginal Means, aka Least-Squares Means.
657 2.0.1 [accessed 2026 Feb 15]. https://CRAN.R-project.org/package=emmeans.
658 https://doi.org/10.32614/CRAN.package.emmeans

659 Lin S et al. 2024. The UBE2J2/UBE2K-MARCH5 ubiquitination machinery regulates apoptosis in
660 response to venetoclax in acute myeloid leukemia. Leukemia. 38(3):652–656 [accessed 2025 Oct
661 5]. https://www.nature.com/articles/s41375-024-02178-x. https://doi.org/10.1038/s41375-024-
662 02178-x

663 Lips C et al. 2020. Who with whom: functional coordination of E2 enzymes by RING E3 ligases
664 during poly-ubiquitylation. The EMBO Journal. 39(22):e104863 [accessed 2021 Apr 26].
665 http://www.embopress.org/doi/full/10.15252/embj.2020104863.
666 https://doi.org/10.15252/embj.2020104863

667 Liu X et al. 2019. Human cytomegalovirus evades antibody-mediated immunity through
668 endoplasmic reticulum-associated degradation of the FcRn receptor. Nat Commun. 10(1):3020
669 [accessed 2025 Oct 5]. https://www.nature.com/articles/s41467-019-10865-y.
670 https://doi.org/10.1038/s41467-019-10865-y

671 Mehrtash AB, Hochstrasser M. 2022. Elements of the ERAD ubiquitin ligase Doa10 regulating
672 sequential poly-ubiquitylation of its targets. iScience. 25(11) [accessed 2025 Oct 5].
673 https://www.cell.com/iscience/abstract/S2589-0042(22)01623-6.
674 https://doi.org/10.1016/j.isci.2022.105351

675 Nakao F et al. 2023. Targeting a mitochondrial E3 ubiquitin ligase complex to overcome AML cell-
676 intrinsic Venetoclax resistance. Leukemia. 37(5):1028–1038 [accessed 2025 Oct 5].
677 https://www.nature.com/articles/s41375-023-01879-z. https://doi.org/10.1038/s41375-023-01879-z

678 Parashar S, Kaushik A, Ambasta RK, Kumar P. 2025. E2 conjugating enzymes: A silent but crucial
679 player in ubiquitin biology. Ageing Research Reviews. 108:102740 [accessed 2025 Oct 2].
680 https://www.sciencedirect.com/science/article/pii/S1568163725000868.
681 https://doi.org/10.1016/j.arr.2025.102740

682 Perez-Riverol Y et al. 2025. The PRIDE database at 20 years: 2025 update. Nucleic Acids Res.
683 53(D1):D543–D553. https://doi.org/10.1093/nar/gkae1011

684 Ravid T, Kreft SG, Hochstrasser M. 2006. Membrane and soluble substrates of the Doa10 ubiquitin
685 ligase are degraded by distinct pathways. EMBO J. 25(3):533–543.
686 https://doi.org/10.1038/sj.emboj.7600946

687 Robinson MD, McCarthy DJ, Smyth GK. 2010. edgeR : a Bioconductor package for differential
688 expression analysis of digital gene expression data. Bioinformatics. 26(1):139–140 [accessed 2026
689 Jan 19]. https://academic.oup.com/bioinformatics/article/26/1/139/182458.
690 https://doi.org/10.1093/bioinformatics/btp616

691 Santos A et al. 2022. A knowledge graph to interpret clinical proteomics data. Nat Biotechnol.
692 40(5):692–702 [accessed 2025 Oct 5]. https://www.nature.com/articles/s41587-021-01145-6.
693 https://doi.org/10.1038/s41587-021-01145-6

694 Sato BK, Schulz D, Do PH, Hampton RY. 2009. Misfolded membrane proteins are specifically
695 recognized by the transmembrane domain of the Hrd1p ubiquitin ligase. Mol Cell. 34(2):212–222.
696 https://doi.org/10.1016/j.molcel.2009.03.010

697 Serin EAR, Nijveen H, Hilhorst HWM, Ligterink W. 2016. Learning from Co-expression
698 Networks: Possibilities and Challenges. Front Plant Sci. 7 [accessed 2025 Dec 22].
699 http://journal.frontiersin.org/Article/10.3389/fpls.2016.00444/abstract.
700 https://doi.org/10.3389/fpls.2016.00444

701 Sharninghausen R, Hwang J, Dennison DD, Baldridge RD. 2024. Identification of ERAD-
702 dependent degrons for the endoplasmic reticulum lumen Glick BS, Ron D, editors. eLife.
703 12:RP89606 [accessed 2025 Oct 5]. https://doi.org/10.7554/eLife.89606.
704 https://doi.org/10.7554/eLife.89606

705 Sowa ME, Bennett EJ, Gygi SP, Harper JW. 2009. Defining the human deubiquitinating enzyme
706 interaction landscape. Cell. 138(2):389–403 [accessed 2012 Mar 15].
707 http://www.ncbi.nlm.nih.gov/pubmed/19615732. https://doi.org/10.1016/j.cell.2009.04.042

708 Stewart MD, Ritterhoff T, Klevit RE, Brzovic PS. 2016. E2 enzymes: more than just middle men.
709 Cell Res. 26(4):423–440. https://doi.org/10.1038/cr.2016.35

710 Swarnkar A et al. 2024. Determinants of chemoselectivity in ubiquitination by the J2 family of
711 ubiquitin-conjugating enzymes. The EMBO Journal. 43(24):6705–6739 [accessed 2025 Oct 5].
712 https://www.embopress.org/doi/full/10.1038/s44318-024-00301-3. https://doi.org/10.1038/s44318-
713 024-00301-3

714 Vella D et al. 2017. From protein-protein interactions to protein co-expression networks: a new
715 perspective to evaluate large-scale proteomic data. J Bioinform Sys Biology. 2017(1):6 [accessed
716 2025 Dec 22]. https://bsb-eurasipjournals.springeropen.com/articles/10.1186/s13637-017-0059-z.
717 https://doi.org/10.1186/s13637-017-0059-z

718 Vrentzou A et al. 2025. UBE2J2 sensitizes the ERAD ubiquitination cascade to changes in
719 membrane lipid saturation. Nat Commun. 16(1):8973. https://doi.org/10.1038/s41467-025-64777-1

720 Wang X et al. 2009. Ube2j2 ubiquitinates hydroxylated amino acids on ER-associated degradation
721 substrates. J Cell Biol. 187(5):655–668 [accessed 2025 Oct 5].
722 https://doi.org/10.1083/jcb.200908036. https://doi.org/10.1083/jcb.200908036

723 Weber A et al. 2016. Sequential Poly-ubiquitylation by Specialized Conjugating Enzymes Expands
724 the Versatility of a Quality Control Ubiquitin Ligase. Mol Cell. 63(5):827–839.
725 https://doi.org/10.1016/j.molcel.2016.07.020

726 van de Weijer ML et al. 2014. A high-coverage shRNA screen identifies TMEM129 as an E3 ligase
727 involved in ER-associated protein degradation. Nat Commun. 5:3832.
728 https://doi.org/10.1038/ncomms4832

729 van Wijk SJL et al. 2009. A comprehensive framework of E2–RING E3 interactions of the human
730 ubiquitin–proteasome system. Molecular Systems Biology. 5(1):317 [accessed 2025 Oct 5].
731 https://doi.org/10.1038/msb.2009.76. https://doi.org/10.1038/msb.2009.76

732 van Wijk SJL, Timmers HTM. 2010. The family of ubiquitin-conjugating enzymes (E2s): deciding
733 between life and death of proteins. The FASEB Journal. 24(4):981–993 [accessed 2024 Nov 26].
734 https://onlinelibrary.wiley.com/doi/abs/10.1096/fj.09-136259. https://doi.org/10.1096/fj.09-136259

735 Witus SR et al. 2021. BRCA1/BARD1 site-specific ubiquitylation of nucleosomal H2A is directed
736 by BARD1. Nat Struct Mol Biol. 28(3):268–277 [accessed 2025 Oct 5].
737 https://www.nature.com/articles/s41594-020-00556-4. https://doi.org/10.1038/s41594-020-00556-4

738 Wolf LM, Lambert AM, Haenlin J, Boutros M. 2021. EVI/WLS function is regulated by
739 ubiquitylation and is linked to ER-associated degradation by ERLIN2. J Cell Sci.
740 134(16):jcs257790 [accessed 2025 Oct 5]. https://doi.org/10.1242/jcs.257790.
741 https://doi.org/10.1242/jcs.257790

742 Ye Y, Rape M. 2009. Building ubiquitin chains: E2 enzymes at work. Nat Rev Mol Cell Biol.
743 10(11):755–764 [accessed 2025 Oct 5]. https://www.nature.com/articles/nrm2780.
744 https://doi.org/10.1038/nrm2780

745 Younger JM et al. 2006. Sequential Quality-Control Checkpoints Triage Misfolded Cystic Fibrosis
746 Transmembrane Conductance Regulator. Cell. 126(3):571–582 [accessed 2025 Oct 31].
747 https://linkinghub.elsevier.com/retrieve/pii/S0092867406009081.
748 https://doi.org/10.1016/j.cell.2006.06.041

749 Yu G, Wang L-G, Han Y, He Q-Y. 2012. clusterProfiler: an R Package for Comparing Biological
750 Themes Among Gene Clusters. OMICS: A Journal of Integrative Biology. 16(5):284–287 [accessed
751 2025 Oct 31]. https://journals.sagepub.com/doi/10.1089/omi.2011.0118.
752 https://doi.org/10.1089/omi.2011.0118

753 Yu X et al. 2025. UBE2J2 is essential for the progression of meiosis prophase I during
754 spermatogenesis in mice. iScience. 28(8) [accessed 2025 Oct 5].
755 https://www.cell.com/iscience/abstract/S2589-0042(25)01139-3.
756 https://doi.org/10.1016/j.isci.2025.112878

757 Zattas D, Hochstrasser M. 2015. Ubiquitin-dependent protein degradation at the yeast endoplasmic
758 reticulum and nuclear envelope. Crit Rev Biochem Mol Biol. 50(1):1–17.
759 https://doi.org/10.3109/10409238.2014.959889

760